



Superconductivity of Electrodeposited Sn Films

Q. Huang*,z

Department of Chemical and Biological Engineering, The University of Alabama, Tuscaloosa, Alabama 35487, United States of America

Tin (Sn) films are electrodeposited on Au seed layers for the investigation of superconductivity. The effects of the presence of suppressing additives in electrolyte, the thickness of Sn films, and the room temperature aging of deposited Sn films on the superconducting transition behavior are systematically studied. In addition, the crystallographic structure of electrodeposited Sn and its evolution along with aging time are characterized and are discussed in conjunction with the superconductivity behavior. The current work represents an important step towards the processing of technologically viable superconducting devices.

© 2023 The Electrochemical Society ("ECS"). Published on behalf of ECS by IOP Publishing Limited. [DOI: 10.1149/1945-7111/acc3c6]

Manuscript submitted February 26, 2023; revised manuscript received March 8, 2023. Published March 22, 2023.

As superconducting quantum computers continue to develop, 3D integration using superconducting metal structures would be eventually demanded to enable the access to each individual qubit in a scaled dense array. 1-3 Electrodeposited superconducting structures would naturally become a candidate choice as the copper counterparts have been manufactured using similar approaches for the conventional semiconductor integrated circuits. 4-6 In those processes, organic additives are typically used to tune the Cu growth rates at different locations, resulting in defect free filling of metal structures. Among the superconducting metals, Sn presents a reasonably high superconducting transition temperature, i.e., the critical temperature T_c at 3.7 K, in its crystalline bulk form⁷ and provides good manufacturing compatibility. The electrodeposition of Sn and its alloys has been long studied and various organic additives have been used to tune the growth rate and to control the morphology, appearance, as well as properties of the deposit. 10-1 However, to our best knowledge, the superconductivity of electrodeposited Sn films, particularly in the presence of organic additives, has not been studied. This paper reports a study of the superconductivity of Sn films electrodeposited on Au seed layer and the effect of a suppressing polymer additive, Ethylenediamine tetrakis (propoxylate-block-ethoxylate) tetrol, or abbreviated as ETT, on the superconductivity. The suppressing effect was reported as a result of the physisorption of ETT molecules on Sn electrode surface, which depends on the applied potential, the concentration and hydrophobicity of the polymer molecule.¹²

Experimental

A three-compartment cell is used for the studies. Sn (99.99%) foil is used as the counter electrode placed in anolyte compartment separated from the catholyte with a glass frit. Ag/AgCl with saturated KCl solution is used as the reference connected to the catholyte with a capillary. All potentials in this report are with respect to this reference. A Pt rotating disc electrode (RDE) with diameter of 5 mm is used as the working electrode in electrochemical studies. Silicon coupons with a patterned Au seed layer are mounted on a rotating disc sample holder and are used as the working electrode to prepare films for characterization. The pattern is fabricated as follows. A layer of 50 nm thermal silicon oxide is first grown on Si, UV lithography is used to create the patterns in photoresist, a stack of 5 nm Ta and 100 nm Au is evaporated on the pattern, and the metals on photoresist are lifted off, leaving the Au patterns behind on silicon oxide. The Au pattern comprises a 1 mm by 10 mm strip and a 3 mm by 5 mm contact pad. The coupon holder fits into a PINE rotator and is controlled at 400 rpm. The electrical connection to the Au pattern is made using a front contact pin landing on the contact pad. The pin has a diameter of 2.6 mm

Sn electrodeposition is carried out in an electrolyte comprising 0.15 M SnSO₄ and 1 M H₂SO₄. An organic additive, ETT with molecular weight 7,200, is used to study the effects of suppressing additives on superconductivity. An Autolab 302 N potentiostat with frequency analyzer is used for all the electrochemical studies. The ohmic resistance of electrolyte is determined using a 10-mV sinusoidal voltage with frequency scanning from 100 KHz to 0.1 Hz. A Bruker Mistral X-ray fluorescence (XRF) spectroscope with a 0.7 mm collimator operated at 50 kV 800 μ A is used to determine the average thickness of deposited films. The crystallographic structure of Sn films is characterized using a Bruker D8 powder X-ray diffractometer (XRD) with Co Ka X-ray source (wavelength = 1.79 Å) operated at 40 kV and 40 mA. A Quantum Design Dynacool Physical Property Measurement System (PPMS) is used to measure the film resistance and determine the superconducting transition. Aluminum wires are bonded between the strip pattern and the PPMS puck using Dupont 4929 NTM silver paint to form the 4-probe configuration for measurement. The film resistance is measured at AC mode with the temperature sweeping from 30 K to 10 K at a speed of 3 K min⁻¹ and then from 10 K to 1.7 K at 0.3 K min⁻¹.

Results and Discussion

The electrodeposition of Sn is first studied on Pt electrode using cyclic voltammetry. The solution resistance is measured as 3.9 ohm and the potentials have been corrected for this. Figure 1a shows two CVs on Pt with no agitation with different lower vertex potentials. Sn deposition starts at about $-0.45 \,\mathrm{V}$ and the deposition rate increases drastically once passed this potential. This increase seems to be limited by the transport when no agitation is applied and a current peak is observed. The anodic scan results in a typical stripping current and the stripping charge is approximately the same as the cathodic deposition charge, suggesting an nearly 100% current efficiency for the deposition. Upon the application of 400 rpm rotation, as shown in Fig. 1b, the cathodic current increases even much more rapidly, resulting in a large amount of deposition and stripping charges. No steady state anodic current is observed suggesting that the anodic charge results from the anodization and dissolution of Sn into Sn²⁺ and no further oxidation to Sn⁴⁺ occurs at the potentials used. A hysteresis in the cathodic current is also observed, where the potential for Sn deposition on Sn is slightly more positive than on Pt, suggesting a small nucleation overpotential on Pt. The deposition is almost completely suppressed upon the addition of 100 ppm ETT. A small deposition current density below -1 mA cm⁻² is observed even at a much negative potential in contrast to -200 mA cm⁻² in the additive free case. A detailed investigation on the adsorption and suppression effect of ETT on Sn electrodeposition has been reported separately, 14 while the brief

including TeflonTM coating, resulting in the exposed Au electrode surface for deposition at $0.197~\rm cm^2$, almost identical with the surface area of the 5 mm Pt RDE.

^{*}Electrochemical Society Member.

^zE-mail: qhuang@eng.ua.edu

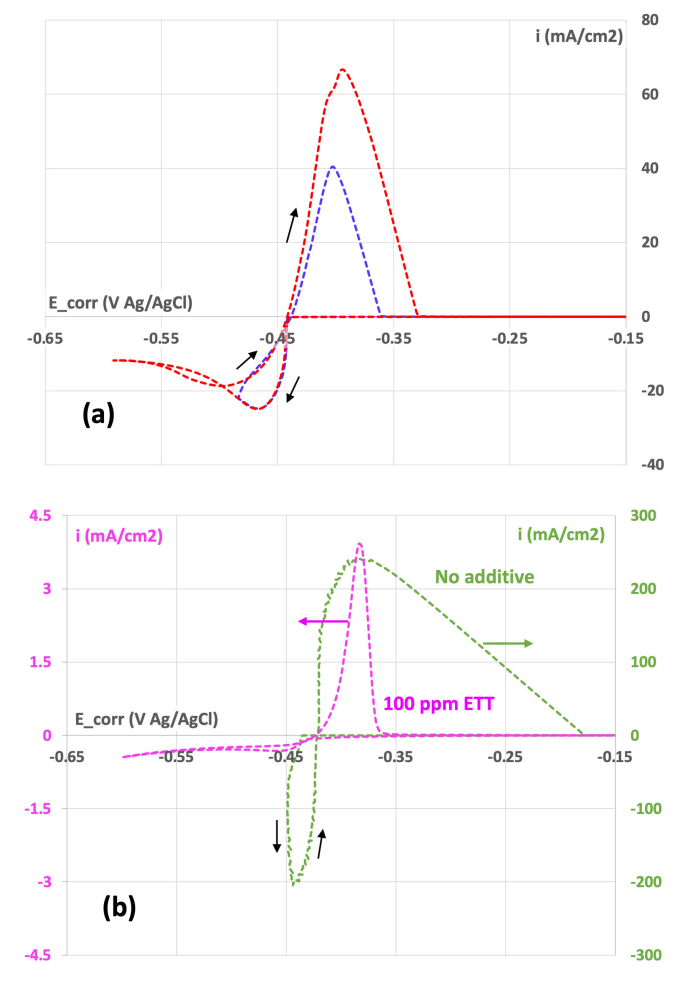


Figure 1. Cyclic voltametry of Sn deposition on Pt RDE (a) with no rotation and no additive; and (b) at 400 rpm with and without ETT. The black arrows represent the sweep directions.

observation here motivates our interest in their effects on the film superconductivity.

Galvanostatic deposition studies have also been conducted at different current densities, where the Sn films are anodically stripped afterwards using linear sweep voltammetry. The anodic charge obtained in those studies are found very similar to the cathodic deposition charge, confirming a nearly 100% efficiency in Sn deposition. This is true for current densities from -5 to -50 mA cm⁻² and rotation rates from 400 to 1000 rpm, even in the presence of 500 ppm ETT. The current efficiency quickly decreases when the current density goes beyond -60 mA cm⁻² at a lower rotation rate of 400 rpm, due to the mass transport limitation of Sn. Because the cathodic current density remains under 1 mA cm⁻² in the presence of ETT in Fig. 1b, the mass transport does not play a role here and the current efficiency remains 100%. In other words, the current decrease observed in Fig. 1b upon the addition of ETT reflects the suppression effect on Sn deposition rate.

Figure 2 shows the superconducting transition of two Sn films deposited on Au pattern substrates without and with ETT additive in the electrolyte. The film in Fig. 2a is deposited without additive at -50 mA/cm^2 for 100 seconds, equivalent to a thickness of 4.2 μ m with 100% efficiency. However, the thickness determined with XRF is 1.5 μ m, suggesting a much lower current efficiency when deposition is conducted on the Au pattern coupons mounted on a holder. The deposition on an ideal RDE electrode at -50 mA/cm^2 showed 100% efficiency as discussed previously. The decreased efficiency reflects a mass transport limitation of Sn, resulting in a more negative potential needed for the applied current density in this

study and therefore a higher hydrogen evolution reaction. While more detailed studies are needed to understand the reason, it is believed that the front contact pin significantly changes the local hydrodynamics on coupon suface, decreases the mass transport of Sn cations, and lowers the current efficiency. The film resistance gradually decrases upon cooling and shows a sudden drop at 3.68 K. However, it does not drop to zero but rather by a very small percent. On the other hand, Fig. 2b presents the same measurement for a Sn film deposited with 500 ppm ETT at a similar current density of -40 mA cm^{-2} , with a thickness of $0.78 \mu \text{m}$ determined by XRF. It is thinner than the film without additive in 2(a) but presents a sharp transition to a superconducting state, namely, zero resistance, at an approximately same critical temperature of 3.3 K.

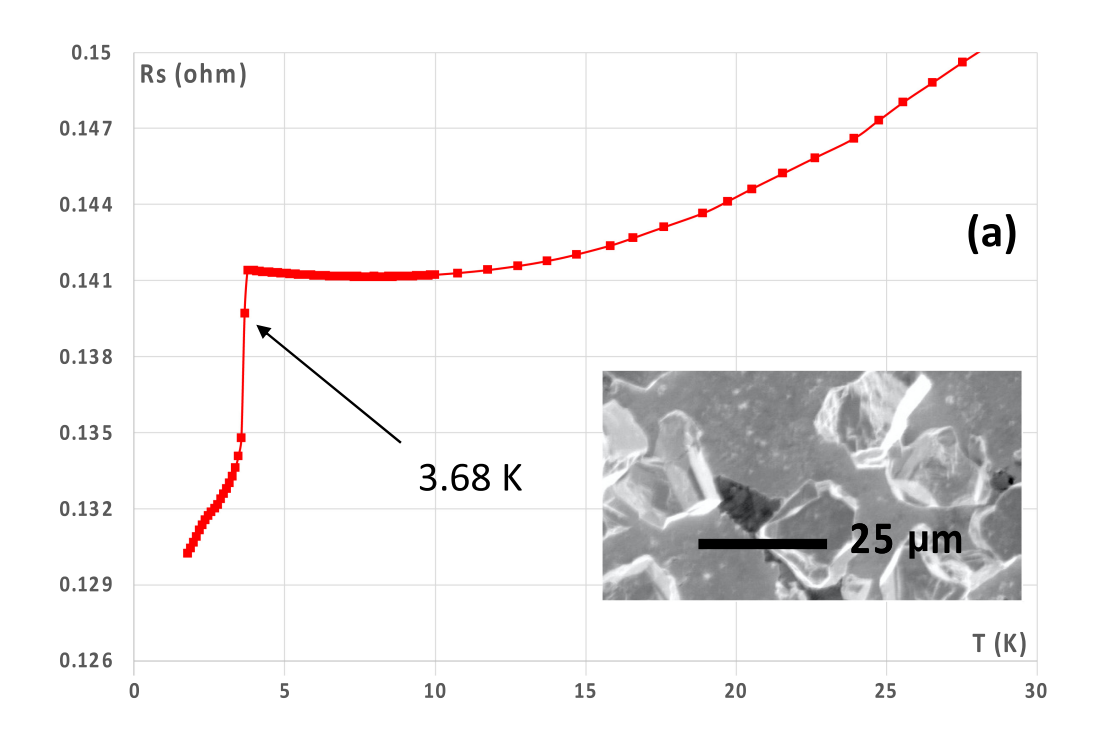
Electrodeposited Sn without additives has been reported to grow as big islands. ¹⁵ This is consistent with the observation in the insets of Figure 2. While the Sn can be superconducting, they are not completely connected. Therefore, the resistance measured with 4-probe configuration includes large portion of the behavior of the Au seed. On the other hand, the suppressing ETT is shown to significantly improve the nucleation of Sn on Au and promote the coalescence of the Sn film. Therefore, a continuous Sn film presents the sharp transition. A small difference is observed between the two T_c's, where the continuous Sn film requires slightly lower temperature to become superconducting. This is believed to relate to the thickness difference between the two films, which will be discussed later.

Figure 3a shows a study of the effects of film thickness on the superconducting transition. 500 ppm ETT is used across all film deposition in order to exclude the uncertainty about the coalescence of film. The four films are deposited at -20 mA/cm^2 for 1, 2, 3, and 10 min, respectively. The film thickness measured with XRF are 34, 119, 174, and 596 nm, respectively, also much thinner than the estimation based on Pt RDE. The film resistance shown in Fig. 3a has been normalized with the resistance at 10 K for easy comparison between different films. The 10-min film showed a sharp transition to the superconduciting state with a T_c of 3.45 K. While such sharp transition is still largely present for a thinner film deposited for 3 min, a sluggish tail in the transition is observed suggesting a significant portion of the deposited film has a lower T_c of 2.6 K. This sluggish transition becomes more dramatic as the film thickness further decreases. Finally, such superconducting transition is not observed at all for the thinnest Sn film deposited for only 1 min.

X-ray diffraction is performed for these four films to characterize their crystallographic phases, and the results are presented in Fig. 3b. The standard XRD patterns for metals and compounds are computed using PowderCell software and Pearson's crystallographic structure data. 16 The thickest 10-min film showed four strong Sn peaks, (101), (220), (211), and (301). Among these reflections, the (101) and (301) peaks deminishes for the film deposited for 3 min, and all Sn peaks have completely deminished as the film thinkness further decreases. For the thinnest film deposited for only 1 min, only two peaks of AuSn alloy are observed (other than the Au substrate peak). In other words, all the Sn has been consumed within 4 hours to form this 1:1 bimetalic compounds. On the other hand, as the Sn thickens up, or when more Sn is available, the AuSn peaks decrease and a Sn-richer phase at 2θ at 48.4° increases. Both $AuSn_2$ and $AuSn_4$ have a reflection at this 2θ . As the discussion in the later results in Fig. 4 will show, this reflection is believed to result from AuSn₄ instead of AuSn₂.

These observations in Fig. 3 suggest that the electrodeposited Sn reacts with the Au seed layer at room temperature, resulting in various alloys or compounds depending on the amount of Sn and altering the superconductivity behavior of the deposit. To further investigate this mechanism, the films are aged at room temperature with the superconductivity and crystal structure being monitored.

Figures 4a and 4b show the film resistance and XRD patterns for Sn film deposited for 3 min and aged for different amount of time. While a small tail at superconducting transition is observed 4 h after deposition (same as the results in Fig. 3, considered as measured



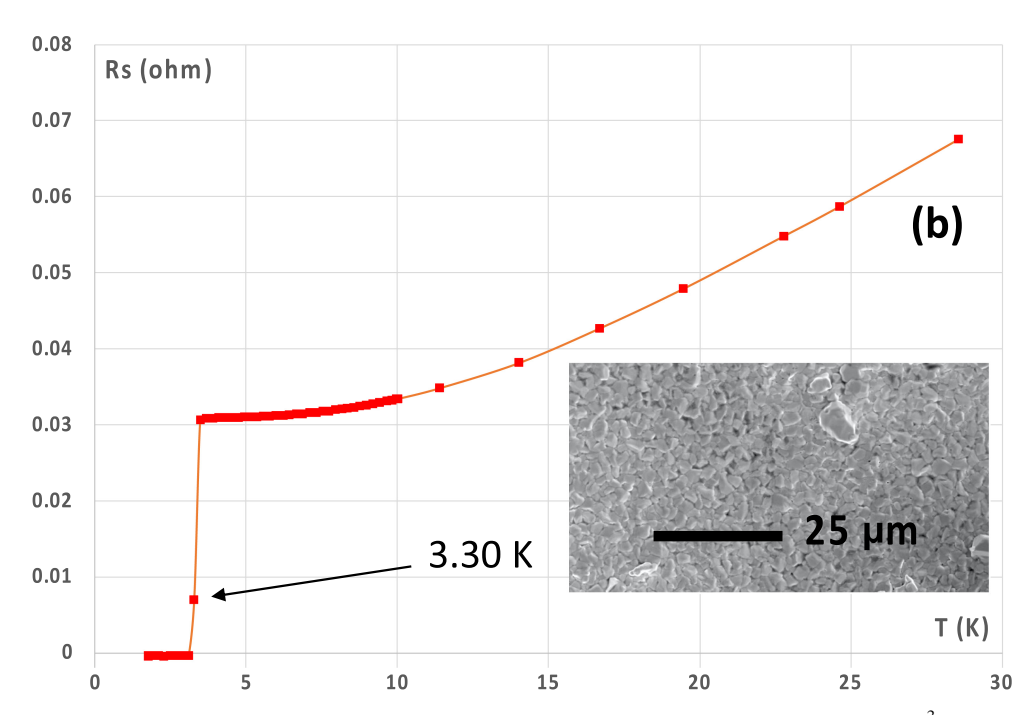


Figure 2. Film resistance measurement along with temperature sweep for (a) Sn film deposited without additive at -50 mA/cm^2 for 100 seconds, and (b) Sn film deposited with 500 ppm ETT at -40 mA/cm^2 for 60 seconds. The insets are the topdown SEM images of two similar films deposited without and with ETT, respectively.

immediately after deposition), this transition is further retarded after being aged for 1 day. No complete superconducting state is achieved beyond 1.7 K after aging for 2 days. While the film still presents some decrease in resistance starting from 3.2 K after 1 week of aging, this decrease is less than 20%, suggesting a majority portion of the film does not become superconducting beyond 1.7 K.

No peaks of pure Sn is observed anymore on XRD patterns after 1 day. On the other hand, the reflections from AuSn and AuSn₂ phases continuously increase. Both phases are present and dominate the film even after 1 week. It is interesting to see that the peak at 2θ

at 48.4° grows at the beginning, decreases afterwards, and completely diminishes after 2 days. At the same time, the other $AuSn_2$ peaks continuously grow. Therefore, it is believed that this peak represents a Sn-richer $AuSn_4$ phase, which grows in the expense of pure Sn and decreases when it further reacts with Au to form other Au-richer phases. It is also worth noting that pure Au and $AuSn_2$ phases coexist after 1 week, suggesting that the reaction between them to form AuSn is relatively slow and $AuSn_2$ is a relatively stable phase at room temperature. Since the film resistance after 1 week aging still drops at a temperature of 3.2 K albeit gradually, it is

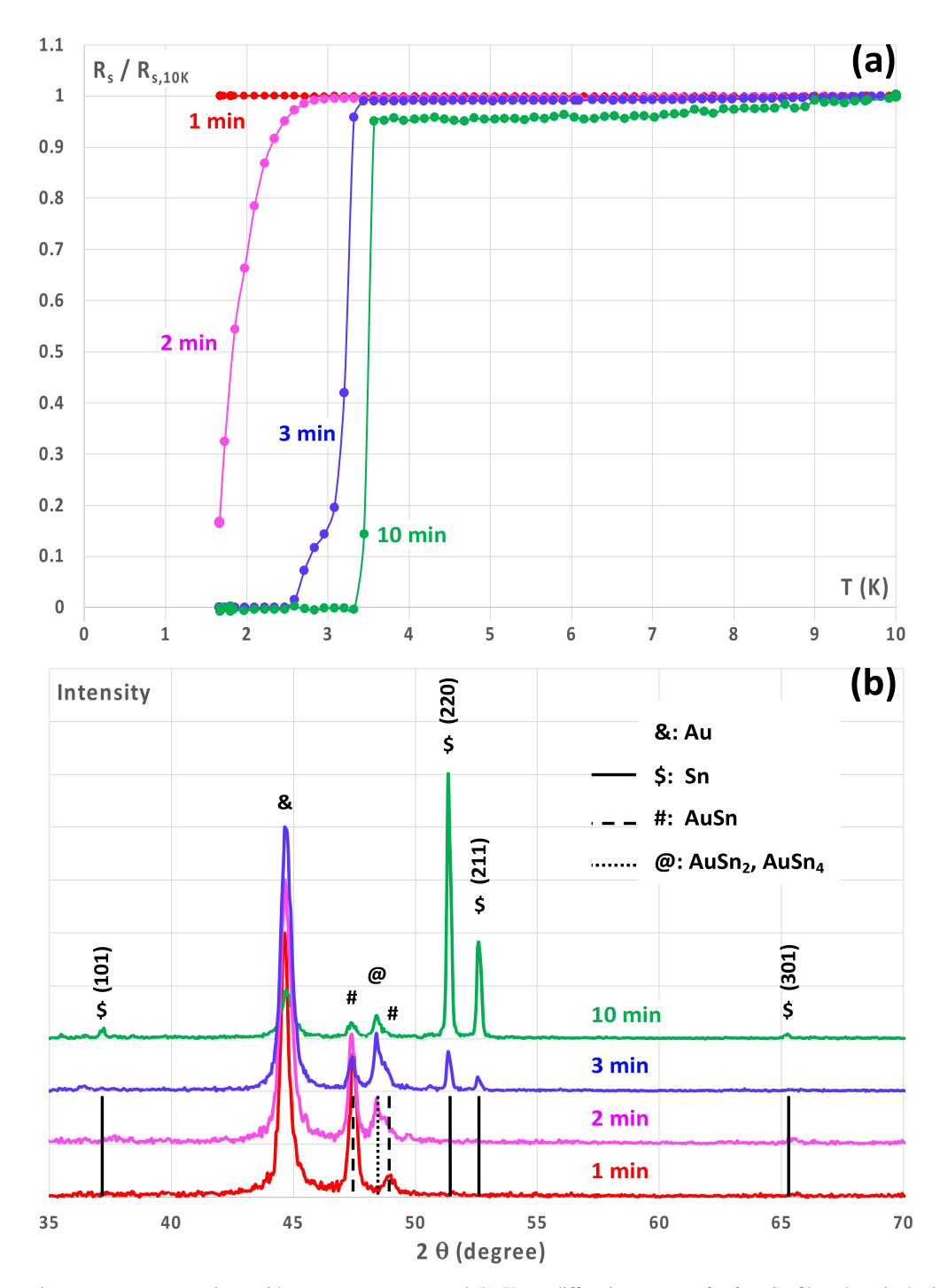


Figure 3. (a) Film resistance measurement along with temperature sweep and (b) X-ray diffraction patterns for four Sn films deposited with 500 ppm ETT at -20 mA/cm^2 for different times. The positions of some relavent Sn and alloy peaks are shown to guide the observation. The film resistance has been normalized with the value obtained at 10 K.

believed that there is very small amount of pure Sn phases even after the 1 week aging although the amount is so small that no Sn peak can be observed in XRD.

A closer look at the film resistance transients shows that, in addition to the transition at intrinsic T_c at 3.4 K, the film can show two additional T_c 's at 2.6 and 1.7 K, respectively. The film aged for 4 h only show one additional transition while the film aged for 1 day show both. Further studies will be needed to confirm this, but the XRD results suggest these different T_c 's might correspond to S_n , S_n and S_n , respectively. While these phases are still present

in films with longer aging, the growth of significant portion of AuSn phase disrupts a continous connectivity between these phases and prevents the observation of a complete superconducting state.

Figures 4c and 4d show the same studies for a thicker Sn film deposited for 10 min The superconducting transition and T_c have remained unchanged after 1 week aging. For brevity, the transitions for shorter aging time in between are not presented as they lay on top of each other. As shown in the XRD patterns, the Au seed layer has been completely consumed by Sn to form bimetallic compounds. On the other hand, a significant portion of pure Sn phase remains in the

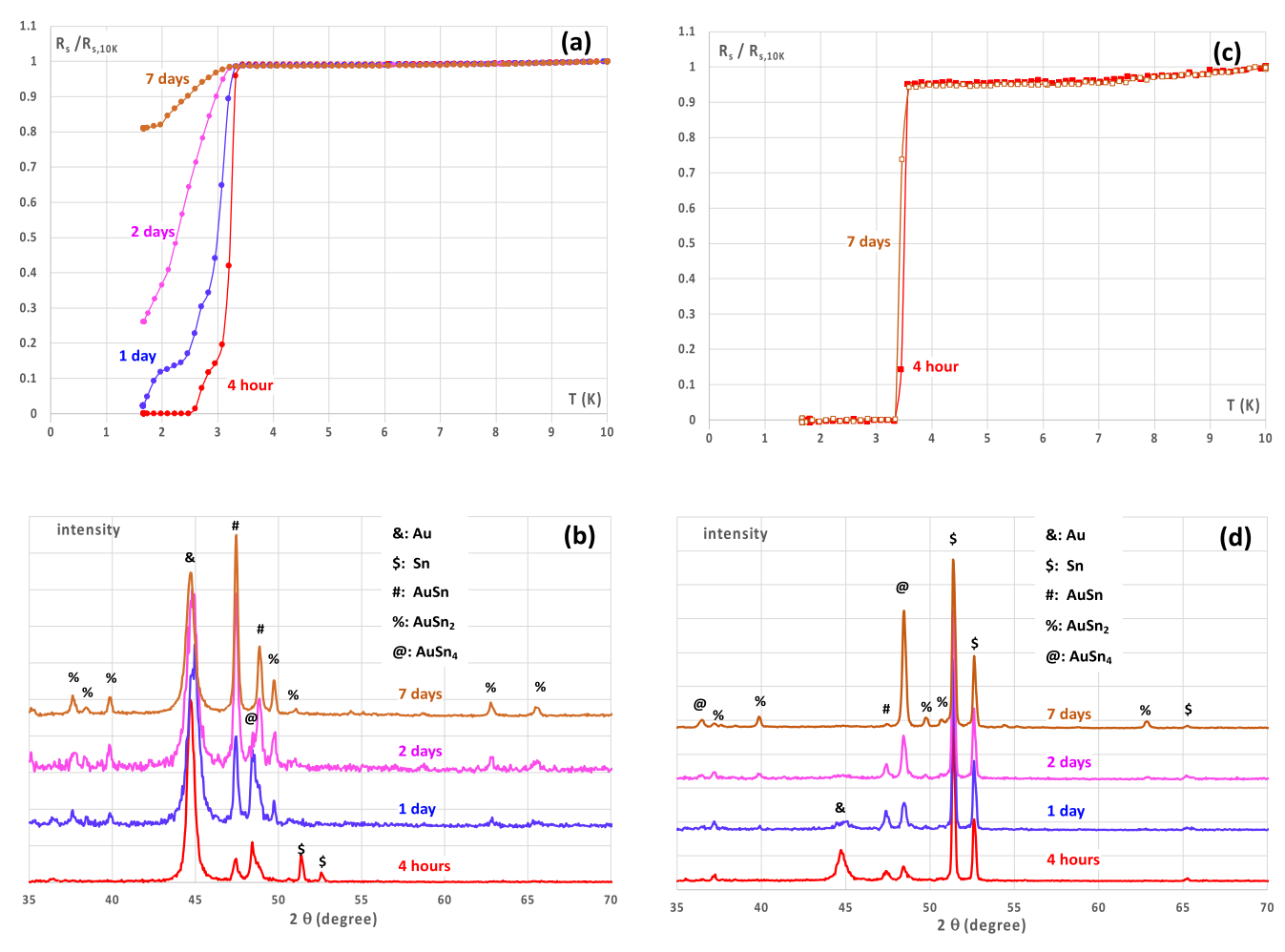


Figure 4. (a,c) Film resistance measurement along with temperature sweep and (b), (d) X-ray diffraction patterns for Sn films deposited with 500 ppm ETT at -20 mA/cm² for (a), (b) 3 min and (c), (d) 10 min and aged at room temperature for different amount of time. The film resistance has been normalized with the value obtained at 10 K.

film even after 1 week, consistent with the $T_{\rm c}$ observation. In addition, among all the bimetallic compound phases, $AuSn_4$ is the dominant one and other Au-richer phases remain minimum.

To summarize the observations, the formation of AuSn takes place immediately upon the deposition of Sn. This is evidenced by the presence of AuSn XRD peaks in Fig. 3b for films only 4 hours after the deposition regardless of the Sn film thickness. When a slightly thicker Sn film is deposited, an additional phase of AuSn₄ forms, suggesting fast diffusion of Au into Sn and a faster formation of AuSn₄ instead of AuSn₂. However, upon aging at room temperature, as shown in Fig. 4b, this AuSn₄ phase grows first and then decreases again. The increase at the early time confirms the fast diffusion of Au into Sn and faster formation of AuSn₄. The decrease at later time happens together with an increase of both AuSn₂ and AuSn phases, suggesting a conversion of AuSn₄ into these Au-richer phases. For a much thicker Sn film in Fig. 4d, a slow reverse reaction appears to take place, converting AuSn back into AuSn₄. However, the AuSn₂ does not react with Sn to form AuSn₄ within the timeframe studied.

Rapid room temperature diffusion during electrodeposition has been reported before, where the low melting metals such as In and Ga are electrodeposited on Cu substrates. ^{17,18} In those cases, the higher melting point metal, Cu, diffuses into the low melting metals to form bimetallic compounds. For the Sn deposited on Au, it is also observed that Au diffuses rapidly into the low melting Sn. The standard Gibbs energy of formation ¹⁹ for AuSn, AuSn₂, and AuSn₄ are -30.29, -38.16, and -38.21 kJ mol⁻¹, respectively. The standard Gibbs energy change of different conversion reactions

discussed above can be calculated as follows.

$$Au + Sn \rightarrow AuSn$$
 $\Delta G_{rxn} = -30.29 \text{ kJ/mol}$ [1]

$$Au + 4Sn \rightarrow AuSn_4$$
 $\Delta G_{rxn} = -38.21 \text{ kJ/mol}$ [2]

$$AuSn + 3Sn \rightarrow AuSn_4$$
 $\Delta G_{rxn} = -7.92 \text{ kJ/mol}$ [3]

$$AuSn_2 + 2Sn \rightarrow AuSn_4$$
 $\Delta G_{rxn} = -0.05 \text{ kJ/mol}$ [4]

$$^{1}/_{2}$$
 AuSn₄ + $^{1}/_{2}$ Au \rightarrow AuSn₂ Δ G_{rxn} = -19.05 kJ/mol [5]

1
/₄ AuSn₄ + 3 /₄ Au \rightarrow AuSn $\Delta G_{rxn} = -20.74 \text{ kJ/mol}$ [6]

While these do not provide the kinetic information, the thermodynamic driving forces for different conversion reactions appear to be consistent with the observations discussed above. For example, reaction (4) has little driving force, consistent with the presence of AuSn₂ despite of excessive Sn in Fig. 4d. Reaction (3) has a small driving force, resulting in very slow conversion from AuSn into AuSn₄. On the other hand, the reactions (1) and (2) as well as (5) and (6) are much more favored, all of which are consistent with the rapid formation of or conversion between these compounds.

Conclusions

Electrodeposition of superconducting Sn film is carried out on Au pattern substrates. While the Sn film deposited additive free shows a

sharp but small resistance decrease, the presence of a suppressing additive, ETT, in electrolyte is found to significantly improve the film continuity and a complete superconducting transition is obtained. The effect of thickness and aging of Sn films on the superconductivity is systematically studied. A thick Sn film deposited for 10 min shows a sharp transition with a T_c at 3.45 K, close to the intrinsic T_c of Sn. On the other hand, this transition is hindered to lower T_c as the film thickness decreases, and no superconductivity can be observed at all beyond 1.7 K for a much thinner Sn film deposited only for 1 min. Room temperature aging of the Sn films results in a gradual degradation of the T_c along with the aging for thin films while the T_c remains unchanged for the thick film. Crystallographic characterization reveals that various bimetallic compounds between Au and Sn are formed at room temperature. Three different T_c's at 3.2, 2.6, and 1.7 K appear to correspond to Sn, AuSn, and AuSn₂, respectively. The formation of or the conversion between bimetallic compounds appears consistent with the thermodynamic data of the compounds.

Acknowledgments

This work is supported by National Science Foundation through grants 1941820 and 2016541. The Alabama Analytical Research Center at the University of Alabama is acknowledged for the access and training of equipment for material characterization. The author also thanks Kamal Ahammed for assisting in wire bonding for two of the films for PPMS measurement.

ORCID

Q. Huang https://orcid.org/0000-0002-1391-6531

References

 Y. Yanay, J. Braumüller, S. Gustavsson, W. D. Oliver, and C. Tahan, "Two-dimensional hard-core Bose-Hubbard model with superconducting qubits." npj Ouantum Information, 6, 1 (2020).

- D.-R. W. Yost, M. E. Schwartz, J. Mallek, D. Rosenberg, C. Stull, J. L. Yoder, G. Calusine, M. Cook, R. Das, and A. L. Day, "Solid-state qubits integrated with superconducting through-silicon vias." npj Quantum Information, 6, 1 (2020).
- S. TAMATE, Y. TABUCHI, and Y. NAKAMURA, "Toward realization of scalable packaging and wiring for large-scale superconducting quantum computers." *IEICE Trans. Electron.*, 105, 290 (2022).
- E. Beyne, "The 3-D interconnect technology landscape." IEEE Design & Test, 33, 8
 (2016).
- D. Josell and T. P. Moffat, "Superconformal copper deposition in through silicon vias by suppression-breakdown." J. Electrochem. Soc., 165, D23 (2018).
- T. Moffat and D. Josell, "Extreme bottom-up superfilling of through-silicon-vias by damascene processing: suppressor disruption, positive feedback and turing patterns." J. Electrochem. Soc., 159, D208 (2012).
- 7. W. M. Haynes, *CRC handbook of chemistry and physics.* (Boca Raton, FL)(CRC press) 96th ed. (2015).
- M. H. H. Ishak, M. S. A. Aziz, F. Ismail, and M. Abdullah, "Influence of copper pillar bump structure on flip chip packaging during reflow soldering: a numerical approach." *Microelectron. Int.*, 38, 172 (2021).
- M. Schlesinger and M. Paunovic, *Modern electroplating*. (New York, Wiley) (2011).
 M. Fukuda, K. Imayoshi, and Y. Matsumoto, "Effect of polyoxyethylenelaurylether on electrodeposition of Pb-free Sn–Bi alloy." *Electrochim. Acta*, 47, 459 (2001).
- P. Ozga, "Electrodeposition of Sn-Ag and Sn-Ag-Cu alloys from thiourea aqueous solutions." Arch. Metall. Mater., 51, 413 (2006).
- Y.-D. Tsai, C.-C. Hu, and C.-C. Lin, "Electrodeposition of Sn-Bi lead-free solders: effects of complex agents on the composition, adhesion, and dendrite formation." *Electrochim. Acta*, 53, 2040 (2007).
- Y. Goh, A. Haseeb, and M. F. M. Sabri, "Effects of hydroquinone and gelatin on the electrodeposition of Sn–Bi low temperature Pb-free solder." *Electrochim. Acta*, 90, 265 (2013).
- Y. Hu, K. Ahammed, Q. Liu, R. Williams, and Q. Huang, "Effects of ethylenediamine tetrakis(ethoxylate-block-propoxylate) tetrol on tin electrodeposition." *Electrochim. Acta*, 421, 140476 (2022).
- A. He, Q. Liu, and D. G. Ivey, "Electrodeposition of tin: a simple approach." J. Mater. Sci., Mater. Electron., 19, 553 (2008).
- P. Villars and L. Calvert, Pearson's Handbook of Crystallographic Data for Intermediate Phases. (Cleveland, OH)(American Society of Metals) (1985).
- Q. Huang, K. Reuter, S. Amhed, L. Deligianni, L. Romankiw, S. Jaime, P.-P. Grand, and V. Charrier, "Electrodeposition of indium on copper for CIS and CIGS solar cell applications." *J. Electrochem. Soc.*, 158, D57 (2011).
- S. Ahmed, K. Reuter, Q. Huang, H. Deligianni, L. Romankiw, S. Jaime, and P. Grand, "Electrodeposited Gallium Alloy Thin Films Synthesized by Solid State Reactions for CIGS Solar Cell." J. Electrochem. Soc., 159, D129 (2012).
- I. Barin and G. Platzki, Thermochemical data of pure substances (Weinheim, Germany)(VCH Verlagsgesellschaft mbH) 3rd ed. (1995).